Point-based Medialness for Animal and Plant Identification

Prashant Aparajeya
Goldsmiths, University of London, U.K.
p.aparajeya@gold.ac.uk

Frederic Fol Leymarie
Goldsmiths, University of London, U.K.
ffl@gold.ac.uk

ABSTRACT

We introduce the idea of using a perception-based medial point description [9] of a natural form (2D static or in movement) as a framework for a part-based shape representation which can then be efficiently used in biological species identification and matching tasks. The first step is one of fuzzy medialness measurements of 2D segmented objects from intensity images which emphasises main shape information characteristics of an object's parts (*e.g.* concavities and folds along a contour). We distinguish interior from exterior shape description. Interior medialness is used to characterise deformations from straightness, corners and necks, while exterior medialness identifies the main concavities and inlands which are useful to verify parts extent and reason about articulation and movement. In a second step we identify a set of characteristic features points built from three types. We define (i) an *Interior dominant point* as a well localised peak value in medialness representation, while (ii) an *exterior dominant point* is evaluated by identifying a region of concavity sub-tended by a minimum angular support. Furthermore, (iii) *convex point* are extracted from the form to further characterise the elongation of parts. Our evaluated feature points, together are sufficiently invariant to shape movement, where the articulation in moving objects are characterised by *exterior dominant point*s. In the third step, a robust shape matching algorithm is designed that finds the most relevant targets from a database of templates by comparing the dominant feature points in a scale, rotation and translation invariant way (inspired by the SIFT method [17]). The performance of our method has been tested on several databases. The robustness of the algorithm is further tested by perturbing the data-set at different scales.

Keywords

2D shape analysis, dominant points, information retrieval, medialness representation, shape compression, articulated movement.

1. INTRODUCTION

In this short communication we introduce our proposed 2D shape representation for biological objects (animals and plants) which is inspired by results and techniques from cognitive psychology, artistic rendering and animation and computer vision (Fig. 1.(h)). An artist will often draw different poses of an animal in movement by using various combinations of primitive structures of different
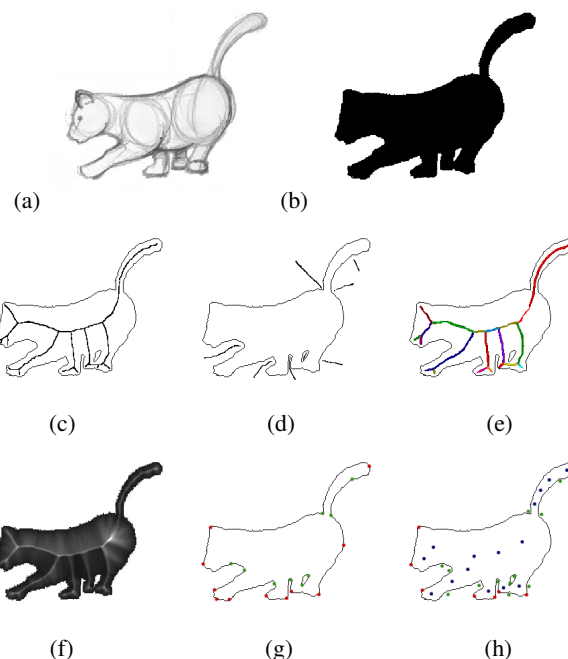
Figure 1: (a) Sketch of a cat built from a small number of approximate disks (visible sketched lines); (b) corresponding segmented and binarised image; (c) classical internal medial-axis approximation; (d) external medial-axis; (e) 2D shock graph; (f) proposed interior medialness map; (g) recovered concave (green dots) and convex (red dots) points, and (h) final dominant (medial) point set (in blue for internal ones, in green for external/concave ones, and in red for convex points) obtained via our method.

sizes (here approximate disks of various radii, Fig. 1.(a)). Different body movements are characterised by a particular orientation and combination of these primitives. From the point of view of psychophysical investigations on the perception of shape movements by humans, Kovács *et al.* have shown that such articulated movements of a biological character can be best captured via a minimal set of dominant features, potentially being represented as isolated points [9].

Inspired with these two approaches to the perception of natural motions, we have investigated a possible scheme based on the notion of robust medialness presented by Kovács *et al.* that can efficiently capture the important structural part-based information commonly used in artistic drawings and animations. The main

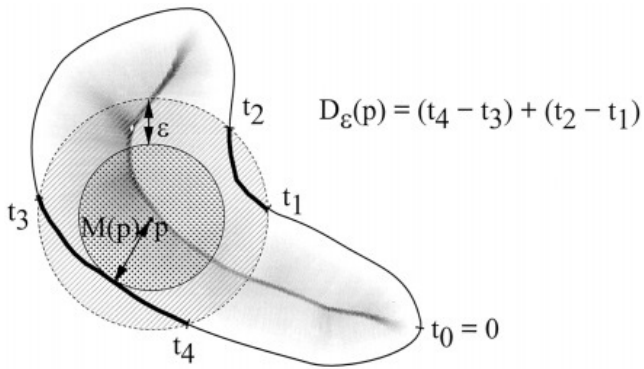$$D_{\epsilon}(p) = (t_4 - t_3) + (t_2 - t_1)$$

Figure 2: From [9, Fig.2] with permission: the D_{ϵ} function for a simple shape defined as an accumulation of curve segments falling inside the annulus neighborhood of thickness ϵ (thick boundary segments within the gray ring) centered around the circle (with center p). $M(p)$ is taken as the minimum radial distance from point p to the nearest contour point.

advantage over other classical medial-based representations of 2D shape is one of combined compactness, robustness and capacity of dealing with articulated movements.

Shape representation towards matching has been addressed in many ways by computer scientists in recent years, including by directly characterising and grouping contour points [24, 15], by contour analysis [2, 10, 5, 21], using Blum's medial axis transform (MAT) and its related shock graph [8], combining contour and skeleton [11, 1], or using instead the inner distance [14] (some of the main medial representations are illustrated in Fig. 1, including our proposed method). Most related to our approach are contour enclosure-based symmetries [7] and medial point transform [22], which compute similar medialness maps, but do not apply these to the retrieval of dominant points and their use in shape matching. Other classical approaches emphasise similarly either boundary information (*e.g.* Fourier, wavelet and scale-space analyses of closed contours) or interior information (*e.g.* primitive retro-fitting or approximation) [18]. The general approach to matching is then to find good ways to put in correspondence the whole shape representation from a query with an equivalent complete shape representation of a target object (*e.g.* extracting a skeleton from a segmented image and defining a process to match it with another skeleton description in the DB). We propose instead to find an efficient medial representation which remains discrete (point-based), is (at least approximately) invariant to scaling, rotations and translations, and can be the basis of a feature vector map for efficient query-target matching tasks as produced in the discipline of Information Retrieval. Note that we do not require to have a complete object segmented and thus will also address partial shape matching. Note also that most of the well established shape-based approaches do not consider deformations and articulated movements, while we do.

Our current method is to develop a shape matching algorithm which is invariant to translation, scale and rotation and is inspired by the now classic SIFT approach [16, 17]. Our shape representation is derived from the region-based medial point description of shape proposed by Kovács *et al.* [9] in cognitive science and perception studies. The purpose of evaluating such medialness measurement is to provide a description of the shape which is local, compact, can easily be applied at different spatial scales, and mimicks human sensitivity to contour stimuli. This process maps the whole shape information into a few number of points we call "dom-

inant" and hence makes it compact. Contrarily to classical medial-based representations, ours is *not overly sensitive* to small boundary deformations and furthermore gives high response in those regions where the object has high curvature with *large boundary support* and in the vicinity of *joints* (between well-delineated parts, such as the limbs of an animal). We augment the medial dominant points with main contour points indicating significant convex and concave features, thus bringing together with our notion of medialness the main 2D point-based shape systems proposed over the years in the fields of cognitive psychology and computer vision: the so-called "codons" denoting contour parts [19] and high curvature convexities often used in scale-space analyses [3].

Mathematically, *medialness* of a point in the image space is defined as the containment of sets of boundary segments falling into the annulus of thickness parameterised by the tolerance value (ϵ) and with interior radius taken as the minimum radial distance of a point from boundary [9] (Fig. 2). On completion of medialness measurements each pixel in the transformed image space holds a local shape information (of accumulated medialness). *Assuming figure-ground separation*, thickness variations, bulges and necks of an object are captured via *interior* medialness measurement. In the work of Kovács *et al.* it is shown that humans are most sensitive to a small number of localised areas of medialness which coarsely correspond to joints for animated bodies [9]. Our equivalent (extended) notion is defined as *dominant points* and can be applied to any objects, animated or not. Dominant points are constrained to be a relatively small number of points of high medialness obtained by filtering out the less informative, redundant and noisy data from the initial medialness image space.

To identify *internal* dominant points a morphological top-hat transform [23] is applied to isolate peaks in the medialness signal. Peaks are filtered using an empirically derived threshold. The selected peaks are then each characterised by a single representative point. To avoid considering large numbers of nearby isolated peaks which are characteristic of object regions with many small deformations, only peaks at a given minimum distance away from each other are retained. The extraction process of *external* dominant point is achieved by combining a concavity measure together with length of support on the contour. Again, a spatially localised filtering is applied to isolate representative dominant points. Furthermore, to improve the robustness of our representation, we extracted the set of *convex points* to capture the blob like structure from the shape. We have observed that the articulation and movement of limbs can be captured via such additional dominant points. Together, the selected dominant points (internal and external) and convex points are then considered as the *representative feature points* of the shape. Our matching algorithm is designed in such a way that it first compares internal dominant points of a query object with internal representative dominant points of target shapes in a database. External dominant points are then similarly processed and convex points are used in a final refinement step. The matching algorithm first analyses the amount of scale, rotation and translation of the query w.r.to the target image. These values are then applied over the query image to find the best possible matching location in the target image.

2. MEDIALNESS MEASURES & FEATURE EXTRACTION

A medial point is defined by computing the D_{ϵ} function as a distance metric (to boundary segments). The D_{ϵ} value at any point in transformed space represents the degree to which this point is associated with a percentage of bounding contour pixels of the ob-
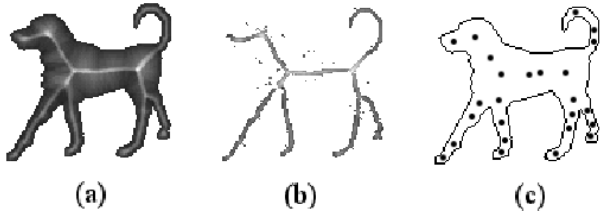
Figure 4: Illustration of the three successive steps in isolating *internal* dominant points: (a) medialness representation of (the interior of) a standing dog figure; (b) corresponding top-hat transform; and (c) internal dominant points illustrated as black dots together with the original object's boundary.

ject within a tolerance of value ϵ (after Kovács *et al.* [9]; Fig. 2). Formally, D_ϵ is defined as: $D_\epsilon(p) = \frac{1}{T} \int_{|p-b| \leq M(p)+\epsilon} db$, for any point $p = [x_p, y_p]$, vector $b(t) = [(x(t), y(t)]$ describing the 2D bounding contour (B) of the object, and normalising factor $T = \int_{b \in B} db$. The metric $M(p)$ is taken as the smallest distance between p and the bounding contour: $M(p) = \min_{0 \leq t \leq 1} |p - b(t)|$. As an example, we performed (interior) medialness measurement on a dog in a typical standing posture to illustrate how the increasing value of tolerance (ϵ) operates an averaging effect on medialness, Fig. 3, as previously observed by Kovács *et al.* [9]: as ϵ increases, smaller symmetries are discarded in favor of those at a larger scale.

2.1 Dominant Points Extraction

Medialness measurement is currently done separately for internal and external regions to take advantage of the perceptual figure-ground dichotomy known to be a powerful cue in humans. This also enables our method to consider articulated objects as potential targets in pattern recognition tasks.

2.1.1 Internal Dominant Points

Medialness increases with "whiteness" in our transformed images (visualisation of medialness). To select points of internal dominance, a "white" top-hat transform is applied, resulting in a series of bright white areas. The white top-hat transform is defined as the difference of an input function (here an image of medialness measures as a grey-level 2D function) with the morphological *opening* of this image by a flat structural element (a disk with radius as a parameter). Opening is a set operator on functions which "removes" small objects from the foreground of an image, placing them in the background (augmenting the local function set values) [23, 6]. This filtering is followed by a thresholding to discard remaining areas of relatively low medialness significance. Figure 4.(b) shows the result obtained after applying the white top-hat transform on a medialness image.

We still require to process further the output of the top-hat transform to isolate the most dominant points amongst the remaining selected medialness points which tend to form clusters. To do so, a flat circular structuring element of radius $\epsilon/2$ (but of at least 2 pixels in width) is applied over the top-hat image such that within the element it produces only that value which maximises medialness. We further impose that no remaining points of locally maximised medialness are too close; this is currently implemented by imposing a minimum distance of length 2ϵ is taken between any pair of selected points. We have found that in practice this is sufficient to avoid the clustering of final interior dominant points (Fig.4.(c)).

2.1.2 External Dominant Points

In practice, if an object can be deformed or is articulated, salient concavities can be identified in association to those deforming or moving areas (such as for joints of a human body). Considering this empirical observation, the location of an external dominant point can be made invariant to this deformation/articulation only up to a certain extent. For example, if the location of an external dominant point is initially relatively far away from the corresponding contour segment, a slight change in the boundary shape near the movable part (such as an arm movement) can considerably change the position of that associated dominant point (Fig. 5, left). On the other hand, if a point is located very close to the contour, it can easily be due to noise or small perturbations in the boundary. Therefore, to be able to retrieve reliable external dominant points, it is first required to provide an adapted definition of concavity as a significant shape feature.
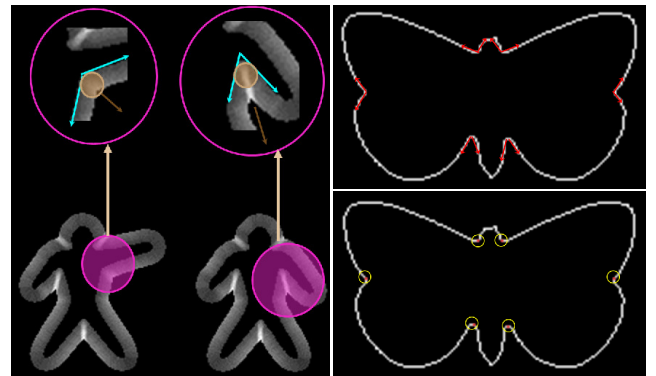

Figure 5: *Left*: External medialness processing on a humanoid. The articulated movement of the left arm changes the location and orientation of the associated external dominant point (at the concave curvature peak). If the external dominant point is reasonably far from the contour, then it proves difficult to retrieve a (shape-based) match with the modified form. Blue arrows show the local support for concavity while brown arrows indicate the direction of flow of medialness (away from the concavity). *Right: Top*: Detection of concave regions (on a butterfly object) using angular support. *Bottom*: Detected Concave points.

We define a point (contour point) of local concavity if it falls under a threshold angular region, under the constraint of length of support which itself depends on the tolerance value (ϵ). The value of threshold (θ) is tunable but is always less than π, which permits to control the angular limit of the concave region. A point whose local concavity is larger than θ is considered a "flat" point. In our experiments we tuned the value of θ from $5\pi/6$ to $8\pi/9$. In association, we define an external circular region (of radius function of ϵ) centered at each locus containing candidate external dominant points. Each such region may provide only one representative dominant point, where the dominance of a particular point is decided by the maximum containment of boundary points inside the associated annulus (of medialness) and corresponds to the maximum length of support. Finally, we position the representative dominant point to be near the contour at a fixed distance outside the form (Fig. 5, right).

2.1.3 Convex Points

Our final shape feature is a set of *convex points*, where a shape has sharp local internal bending and gives a signature of a blob-like
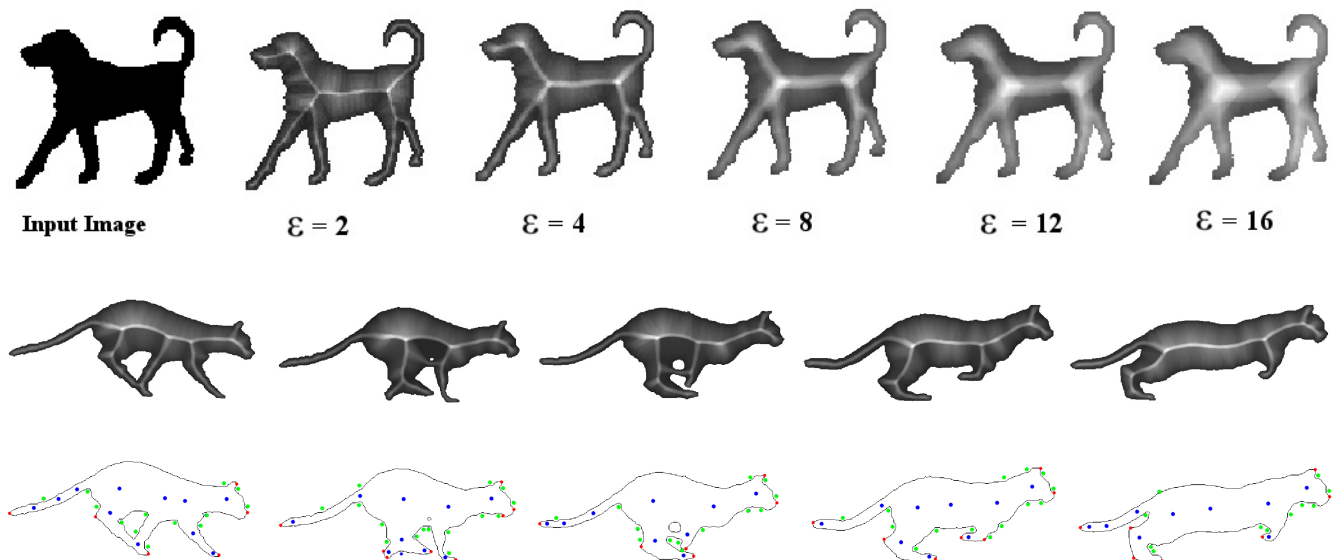
Figure 3: *Top row*: **Medialness and tolerance. Left: A dog standing; other images to the right show variations in D_ϵ for increasing tolerance (ϵ).** *Middle row*: **The D_ϵ-function for a sequential set of frames capturing the profiles of a running leopard. The maxima (white spots) of the function are good candidates as primitives for biological motion representation (after [9]).** *Bottom row*: **Corresponding feature points automatically extracted from the medialness measures visible in the middle row (blue: interior dominant; green: exterior dominant; red: convex points).**

part or significant internal curvature structure (*i.e.* a peak in curvature with large boundary support). The goal is to represent an entire protruding sub-structure using one or a few boundary points. Traditionally, such protrusions have a significant contribution in characterising shape [19, 11, 2, 21]. The process of extraction of convex points is similar to the extraction of concave points, the main difference being the value of threshold angle (θ), where $\pi < \theta \leq 2\pi$. In our experiments we have found useful values to be in the range: $5\pi/4$ to $4\pi/3$. Such convex and concave points are complementary to each others and have been used in the "codon" theory of shape description: a codon is delimited by a pair of negative curvature extrema denoting concavities and a middle representative positive maximum of curvature denoting a convexity [19]. In our case we relate these two sets with the extremities of the traditional medial axis of H. Blum: end points of interior branches correspond to center of positive extrema of curvature and end points of exterior branches are mapped to negative extrema of curvature of the boundary. The repositioning of these extrema near the boundary is alike the end points of the PISA (Process Inferring Symmetry Axis) representation of M. Leyton [13]. Together, the three sets: concave, convex and interior dominant, form a rich enough point-based description of medialness to allow us to efficiently address applications with articulated movement for real image data.

2.2 Articulation

Anatomically, an animal's articulated movement is dependent on the point of connection between two bones or elements of a skeleton. Our results show that exterior dominant points (representative of significant concavities) have higher potential to trace such articulations, unless the shape is highly deformed [12]. For usual movements (*e.g.* walking or jogging), these feature points remain present and identifiable in association to an underlying bone junction and hence can provide a practical signature for it (Fig. 3, bottom).
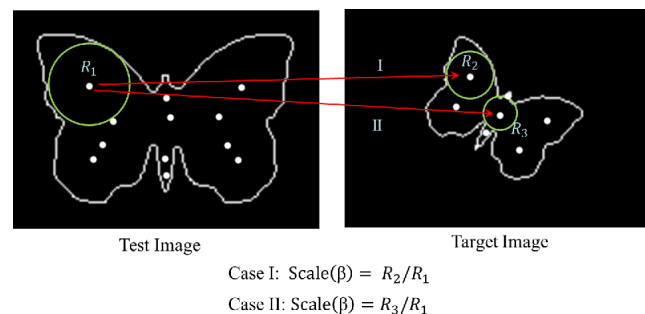
3. MATCHING ALGORITHM

Case I: Scale(β) $= R_2/R_1$
Case II: Scale(β) $= R_3/R_1$

Figure 6: **Illustration of the evaluation of scale (β). In the query image on the left, for a particular dominant point falling inside the green circle, two possible matching locations in the target image, are shown: cases I and II. In each case the circle's radius is dictated by the minimum distance to the contour (from medialness) and the scale (β) is given as the ratio of the minimum radial distances of target vs query.**

Our objective is to design a robust matching algorithm that will match dominant points (query to targets) in an efficient way, in both time (or equivalent numerical complexity) and accuracy. First, both the internal and external dominant points are separately extracted from query and target images. Internal dominant points are the keypoints for evaluating scale, rotation and translation of the query image w.r. to a target image. After finding the scale, rotation and translation of the query image, the next task is to improve the correctness of the matching algorithm. For this, external dominant points can play a role and improve the final accuracy. The following information is associated with the dominant points :

$< X, Y, R, MM >$, where (X,Y) is the 2D location of the dominant point, R is the minimum radial distance of the point from the contour and MM is the medialness measurement. The test case (query Q) is represented as: $Q=\{Q_I, Q_E, Q_c\}$, for internal (Q_I), external (Q_E) dominant points and convex (Q_C) points; while the target image (T) is similarly represented as: $T = \{T_I, T_E, T_C\}$. Each element of Q_I is matched with each element of T_I following four stages.

Stage I finds the scale (β) and translation of the query image by matching a dominant point. Stage II is a check on the scale β to make sure at least one more internal dominant point can be used in the matching process (if not, move to a different dominant point not yet considered). In stage III, the rotation of the query image (w.r.to the target) is evaluated. Finally, stage IV modifies the Cartesian positions of each feature point of the query image by applying the evaluated scale, rotation and translation and we proceed to measure a matching performance value.

Stage I: Take an element (q_i) from set Q_I and match it with each element (t_j) of set T_I. For each pair of (q_i,t_j), the scale (β) is evaluated as: $\beta = \frac{R_{t_j}}{R_{q_i}}$ (Fig. 6). The scale (of query image w.r. to target) for the matching pair (q_i,t_j) is defined via two translations, one for each axial direction: $\overrightarrow{q_x t_x} = t_x - q_x$ and $\overrightarrow{q_y t_y} = t_y - q_y$, where $q_i = (q_x,q_y)$ and $t_j = (t_x,t_y)$.

Stage II: Now take the next element (q_{i+k}) from set Q_I and match it again with each element (t_j) of set T_I. For each pair of (q_{i+k},t_j) find the scale β'. If the ratio of β' over β is under the tolerance level T_s, then goto stage III. Otherwise, repeat at another point and check the same tolerance criterion T_s and repeat if necessary until all the elements of Q_I are counted. The value β' (if it is under the tolerance level) ensures compatibility under scaling of the query image (with respect to a target) and helps in finding the matching location of the next internal dominant point to consider (red arrows in Fig. 7).

Stage III: We define the orientation (α) of an image by the angle between a line joining two matched dominant points (as obtained from step I and II) and the positive (reference) x-axis. If (q_i,q_{i+k}) are the matching dominant points in Q_I and (t_j,t_{j+l}) are matched dominant points in T_I, then orientations α_q and α_t are defined as the angle between matching dominant points (Fig. 7). The rotation (θ) of the image Q is thus defined by the difference of orientations, *i.e.* $rotation(\theta) = \alpha_{T(t_j,t_{j+l})} - \alpha_{Q(q_i,q_{i+k})}$.
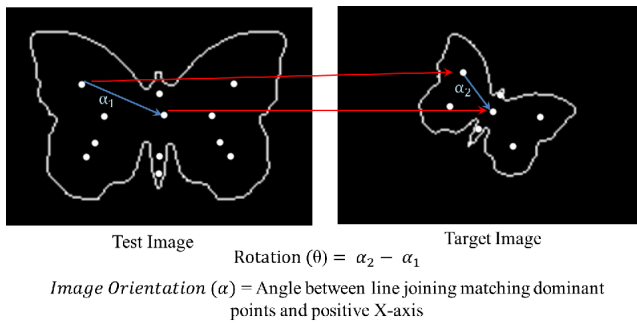

Test Image   Target Image

Rotation (θ) = $\alpha_2 - \alpha_1$

Image Orientation (α) = Angle between line joining matching dominant points and positive X-axis

Figure 7: For both query (test) and target images, the orientation (α) is the angle between a line joining the two matching internal dominant points (shown with blue arrows) and a positive x-axis. The required rotation (θ) of the query image w.r.to the target is given by the difference in orientations.

Stage IV: Upon obtaining the values of translation, rotation and

scale of the image Q (w.r.to T), our next task is to transform the positions of all feature points (Q_I, Q_E and Q_C) of the image Q into the space of image T and finally check for a match. This is done as follows:

1. Construct the 4×4 homogeneous matrix H to perform the required linear (rotation and scaling) and affine (translation) transforms for all feature points found in image Q.

2. Calculate the modified coordinate positions by matrix multiplication of H with the feature point positions.

3. For each modified q_i ($q_i \epsilon Q_I$) if there is a t_j ($t_j \epsilon T_I$) within a tolerance radius of $r \times \epsilon$, their β-value is then compared. If the β ratio is within T_s, then count it as a match.

4. Repeat step 3 for *external* dominant and convex points, *i.e.* each element of Q_E and Q_C with T_E and T_C respectively.

Consider M_I, M_E and M_C as the sets of internally, externally and convex matching feature points. Intuitively, more shape discrimination is present in internal and external dominant points while convex points add details (end points of protruding parts delimited by external (concave) points). Hence we make use of the following heuristic: our matching metric is biased towards internal and external dominant points. We express the problem of finding a best matching location of Q in T as the maximization of the F-measure:

$$F = \frac{2 \times \sum(M_I + M_E)}{\sum(Q_I + Q_E) + \sum(T_I + T_E)} \quad (1)$$

To handle the situations where many F-measures have same values, we then compute a percentage of matched convex points, F_C, and maximize this value. Mathematically,

$$F_C = \frac{2 \times \sum M_C}{\sum(Q_C + T_C)} \quad (2)$$

There is more than one way to combine the information from the three sets of feature points. Currently, we are using first the internal dominant points to reduce the number of targets to further consider for a potential match. Then we add external (concave) dominant points to further reduce the number of candidates, and finally use convex points only if we still have multiple candidates left. Note that we do not use yet in practice additional information implicitly available, such as "codon" structure, *i.e.* how pairs of concavities are associated with specific convex points [19]. This structural information would be useful for finer matching under articulated motions (of limbs). We are currently exploring this combined use of convex points with external dominant points and will report elsewhere on its potential advantage.

4. EXPERIMENTAL RESULTS

Our current matching algorithm is hierarchical in its use of feature points (internal –> external –> convex) and has proven useful even with common body articulated movements, but as pointed out above, this could be refined in the near future by using more structural information. At this early stage in our research program we have performed an extensive experiment on different heterogeneous databases containing biological forms (large animals, plants and insects) to verify the performance in efficiency and accuracy of our novel method. Four main types of datasets were used for this purpose: (i) animals taking a static posture and in movement, (ii) humans taking a static posture or in action (articulated movement), (iii) insects and (iv) plants (only leaf forms currently). Also, we performed some random re-scaling, rotating and translating for the

verification of invariance under such transformations (Fig. 9), and added a number of occlusions, by performing random cuts, to test the method's response beyond affine transforms. Furthermore, the robustness of the algorithm is also evaluated by applying a "structural noise" — introducing scalable random geometric deformations — which we designed by performing randomised morphological set operations on the segmented (binarised) objects. In our experiments we have defined three levels of perturbations: small or less perturbed, medium and large or highly perturbed (examples in Fig. 8). We note that other methods relying on smooth continuous contours (such as methods based on the use of codons or curvature scale-space, as well as many of the traditional medial-axis methods) will have great difficulty in dealing with such deformations — which are to be expected in noisy image captures and under varying environmental conditions such as due to decay and erosion.
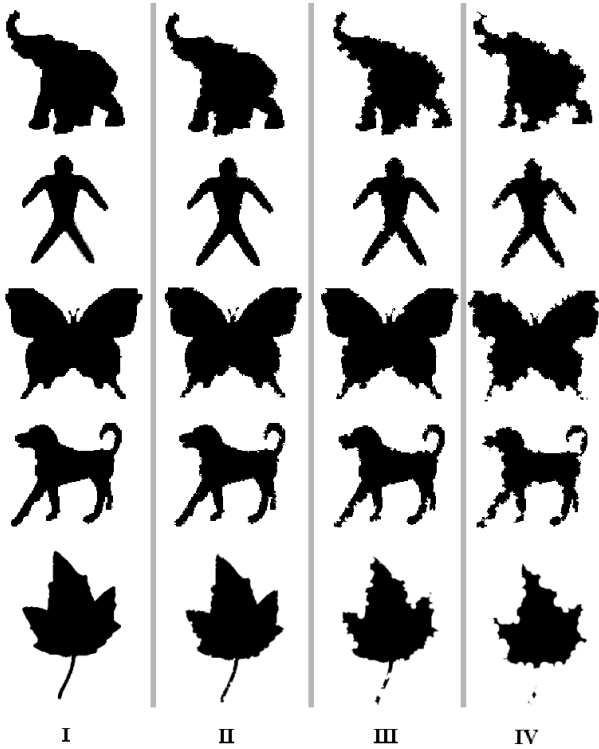
Figure 8: Three levels of (added) perturbation: I - none (originals), II - small , III - medium and IV - large.

To construct different databases we used the standard MPEG-7 [10], ImageCLEF-2013 [4] and Kimia (Brown University's) [20] datasets. Furthermore, we also initiated our own database where we selected different sequences of animals in motion (from videos). From these datasets, we have collected a total of 1130 samples belonging to Animals other than insects (520 samples, including Human, Horse, Rat, Cat, Panther, Turtle, Elephant, Bat, Deer, Dog, and Ray forms), Insects (410 samples, including Butterfly, Bug, Mosquito, Ant, and other miscellaneous insect forms), and Plant leaves (200 samples, including Acercampestre, Aceropalus, Acerplatanoides, Acerpseudoplatanus, Acersaccharinum, Anemone-hepatica, Ficuscarica, Hederahelix, Liquidambarstyraciflua, Liriodendrontulipifer, and Populusalba specimens).

We note that we are limiting the sizes of our test databases as we require well segmented binary forms (distinguishing figure from ground) to initiate our medialness transform (*e.g.* ImageCLEF in-
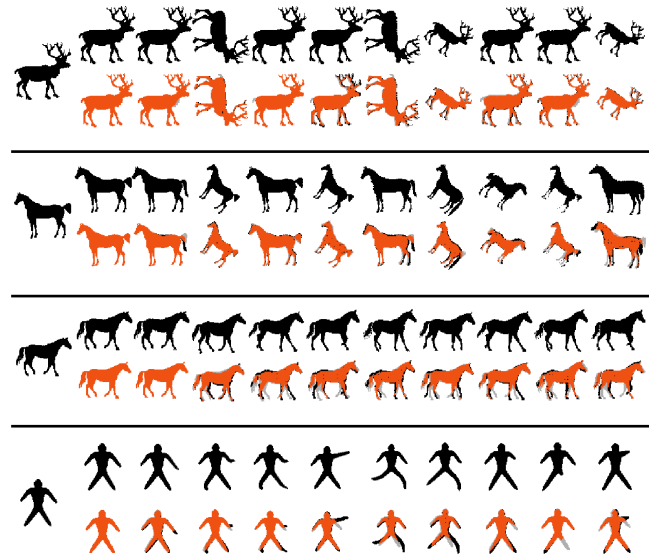

Figure 9: Top-10 results on some of the samples for deer, horse and humanoid forms when using our $F - measure$ as the basis for ranking. The leftmost image for each ranking results is the query, while the images on the top row are the target images matched at successive rank location from best to worst. The bottom row then shows the overlaying (in orange) of the query on the respective target image (after transformation) and their spatial differences. The top two series shows tests for the invariance under scaling, rotation and translation. The third and fourth series show the behavior of matching using the $F - measure$ in the presence of articulated movements.

cludes circa 5000 plant images, while we have segmented only 200 of these thus far). This is a limitation of our current approach, but we are working on extensions to grey-level and color images (as non-segmented inputs). Also, rather than focus on one type of biological forms, say butterflies, we decided to test and show the potential power of our approach for a number of very different biological forms, from plant leaves, to various species of insects to larger animals (including humans).

Furthermore, to check the robustness of our algorithm, we deformed each such sample at the previously indicated three levels of perturbation, thus bringing our total dataset count to $1130 \times 4 = 4520$. From this database, we took each sample as a different query, resulting in a total comparison set of $4520 \times 4520 \approx 20.43$ million forms, and exploited our current ranking metric (F alone, or with F_C) to find the returned top-10 matches. Examples of such top-10 results can be seen in Figures 9, 10, 11, and 12. In our experiments, the matching algorithm always finds the best fitting shape area for the query in the target image (Fig. 13). For empirical analysis, we performed two individual comparisons: (a) precision obtained on different sets of data types (Fig. 14), and (b) precision obtained at different perturbation levels (Fig. 15). When the query image belongs to the original set, the retrieval rate at different ranks is very high, while the performance significantly decreases for high levels of perturbations. Note however that even under a large structural perturbation a given form which may have lost some of its significant shape features (*e.g.* a limb), can still be matched with perceptually similar targets — as judged by a human observer and validated here as we know the ground truth.
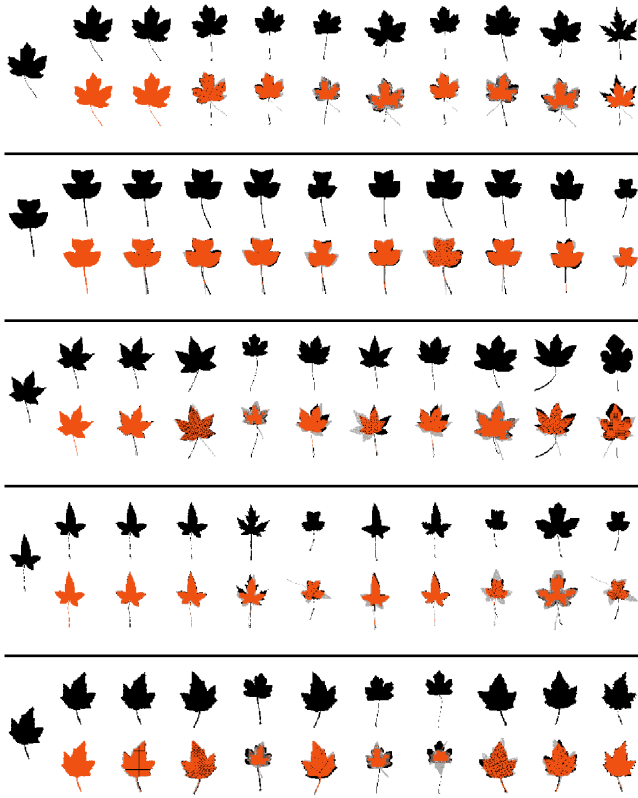
Figure 10: Top-10 results on some of the samples from the *Plant* database (ImageCLEF-2013 [4]) *with shape perturbations* using our $F - measure$ as the basis for ranking. NB: The first match is always the desired target.
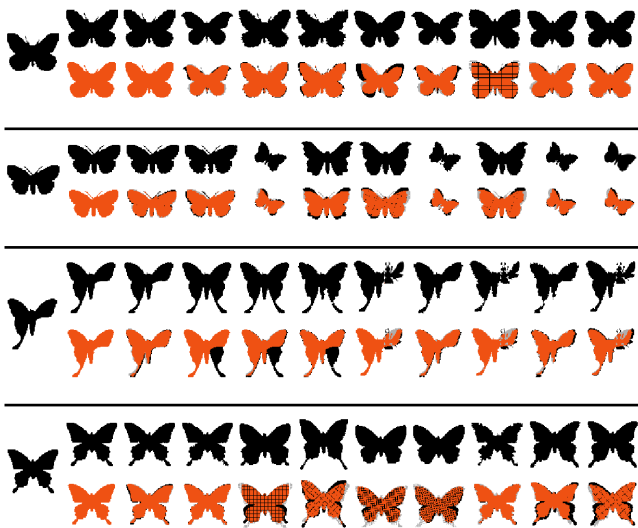

Figure 11: Top-10 results on some of the samples for *butterfly* forms from the *Insect* database including structural perturbations when using our $F - measure$ as the basis for ranking. NB: A partial shape query (3rd series from the top) returns valid and interesting results.
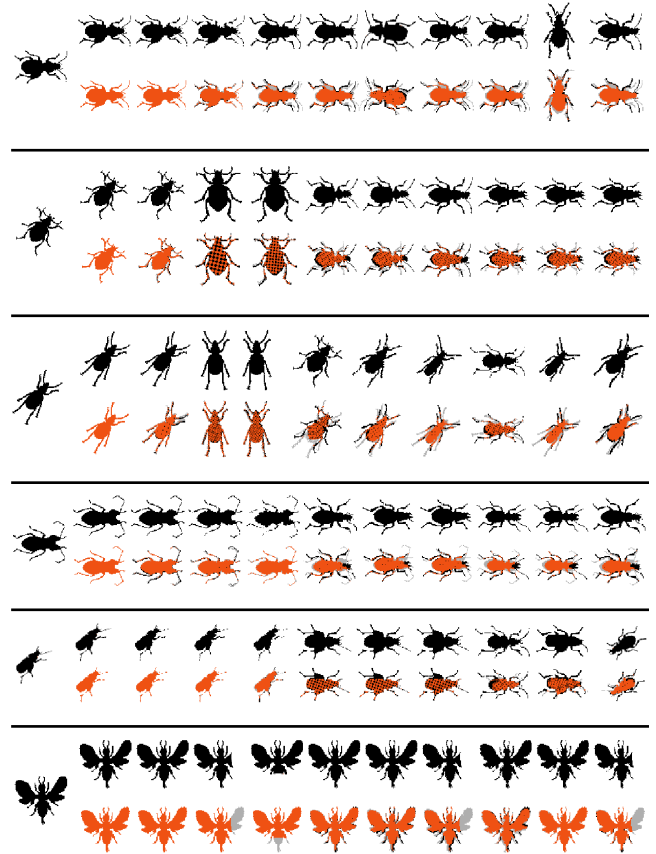

Figure 12: Top-10 results on some of the samples from the *Insect* database including structural perturbations when using our $F - measure$ as the basis for ranking.
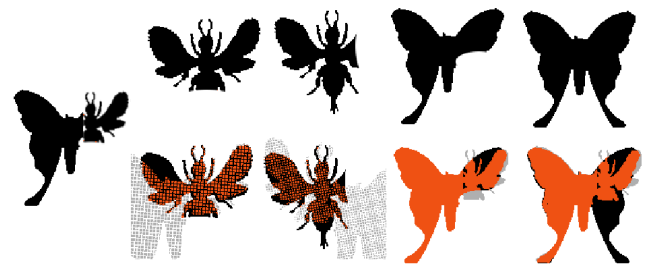

Figure 13: A special query image obtained as a juxtaposition of two different insect cuts finds a best fitting location in the target image, and results into an interesting series of part-based matches (retrieving the correct pair of individual insects (before juxtaposition) from the DB).
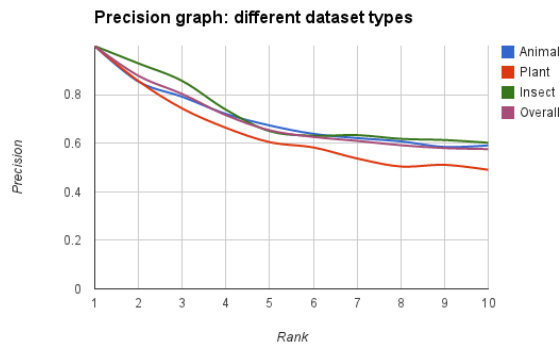
Figure 14: Result analysis (precision) on the different datasets containing originals of large animal, plant and insect images, using our proposed $F - measure$ as the ranking metric.
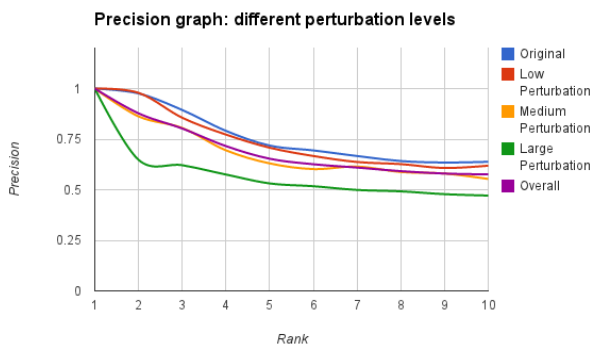

Figure 15: Result analysis of the entire dataset for different levels of perturbations, using our $F - measure$ as the ranking metric. NB: Most of the images are also randomly rotated, scaled and translated.

5. CONCLUSION

The strengths of our approach include: (1) emphasizing a representation of 2D shapes based on results from studies on human perception via robust medialness analysis; (2) introducing an algorithmic chain providing an implementation of this shape analysis tested on current reference 2D binary animal and plant databases; (3) mapping of the whole form into a small number of dominant feature points; (4) achieving accuracy for top ranked matches (exactness) and with nice (observable) degradation properties for the following highest ranking results; (5) testing and demonstrating robustness under some levels of articulation and other structural (noise, cuts) perturbations. Our method also shows promising results for part-based matching tasks, in the context of occlusions, cuts and mixed object parts, as well as for shape reconstruction and compression, all important topics which will require further investigations.

Acknowledgments

6. REFERENCES

[1] X. Bai, W. Liu, and Z. Tu. Integrating contour & skeleton for shape classification. In *ICCV Workshops*, pages 360–7, 2009.

[2] S. Berretti, A. Del Bimbo, and P. Pala. Retrieval by shape similarity with perceptual distance and effective indexing. *IEEE Trans. on Multimedia*, 2(4):225–39, 2000.

[3] M. Bober and F. Mokhtarian. *Curvature Scale Space Representation*. Springer, 2003.

[4] B. Caputo et al. Imageclef 2013: the vision, the data and the open challenges. In *Information Access Evaluation*, pages 250–68. Springer, 2013.

[5] L. Chen, R. Feris, and M. Turk. Efficient partial shape matching using Smith-Waterman algorithm. In *CVPR Workshops*, pages 1–6, 2008.

[6] E.R. Dougherty and R.A. Lotufo. Hands-on morphological image processing. SPIE, 2003.

[7] M. Kelly and M. D. Levine. Annular symmetry operators. In *ICCV*, pages 1016–21, 1995.

[8] B.B. Kimia. On the role of medial geometry in human vision. *Journal of Physiology-Paris*, 97(2):155–90, 2003.

[9] I. Kovács, Á. Fehér, and B. Julesz. Medial-point description of shape. *Vision research*, 38(15):2323–33, 1998.

[10] L. J. Latecki and R. Lakamper. Shape similarity measure based on correspondence of visual parts. *IEEE PAMI*, 22(10):1185–90, 2000.

[11] F. Leymarie and M. D. Levine. Simulating the grassfire transform using an active contour model. *IEEE PAMI*, 14(1):56–75, 1992.

[12] F. Fol Leymarie et al. Point-based medialness for movement computing. In ACM Proc. of MOCO, pp.31–6, Paris, France, 2014.

[13] M. Leyton. *Process Grammar*. Springer, 2012.

[14] H. Ling and D. Jacobs. Shape classification using the inner-distance. *IEEE PAMI*, 29(2):286–99, 2007.

[15] Z. Liu and Meng F. An, J. A robust point matching algorithm for image registration. In *ICMV*, volume SPIE 8350, 2011.

[16] D. G. Lowe. Object recognition from local scale-invariant features. In *ICCV*, volume 2, pages 1150–7, 1999.

[17] D.G. Lowe. Distinctive image features from scale-invariant keypoints. *Int'l J. of Computer Vision*, 60(2):91–110, 2004.

[18] Y. Mingqiang et al. A survey of shape feature extract. tech. In *Pattern Rec. Tech. & Applic.* pp. 43–90, InTech, 2008.

[19] W. Richards and D. D. Hoffman. Codon constraints on closed 2D shapes. *CVGIP*, 31(3):265–81, 1985.

[20] T. Sebastian et al. Recognition of shapes by editing their shock graphs. *IEEE PAMI*, 26(5):550–71, 2004.

[21] P. Srestasathiern and A. Yilmaz. Planar shape representation and matching under projective transformation. *CVIU*, 115(11):1525–35, 2011.

[22] G.J. van Tonder and Y. Ejima. Flexible computation of shape symmetries within the max. disk paradigm. *IEEE SMC, Part B*, 33(3):535–40, 2003.

[23] L. Vincent. Morphological grayscale reconstruction in image analysis. *IEEE Trans. on Ima. Process.*, 2(2):176–201, 1993.

[24] P. B. Van Wamelen et al. A fast expected time algorithm for the 2-D point pattern matching problem. *Pattern Recognition*, 37(8):1699–711, 2004.